Sensors & Transducers, Vol. 217, Issue 11, December 2017, pp. 28-35

www.sensorsportal.com

Sensors & Transducers

Published by IFSA Publishing, S. L., 2017
http://www.sensorsportal.com

W/$FeSb_2$/W Heterostructure for Single-Photon Detection in a Wide Range of Electromagnetic Spectrum

Armen KUZANYAN
Institute for Physical Research, Laboratory of Materials Science, Ashtarak-2, Ashtarak 0203, Republic of Armenia
Tel.: +37494170406, +37410288150
E-mail: akuzanyan@yahoo.com

Received: 14 October 2017 /Accepted: 14 November 2017 /Published: 30 November 2017

Abstract: The results of computer simulation of heat distribution processes taking place after the absorption of single photons of 1 – 1000 eV energy in the three-layer detection pixel of the thermoelectric detector are being analyzed. Different geometries of the detection pixel with thermoelectric sensor made of strongly correlated semiconductor $FeSb_2$, tungsten absorber and heat sink are considered. It is concluded that such detector may register individual photons from IR to X-ray providing energy resolution of not less than 1 % and terahertz counting rate.

Keywords: Thermoelectric single-photon detector, Computer simulation, Three-layer detection pixel, $FeSb_2$ sensor, Tungsten absorber and heat sink.

1. Introduction

The past 20 years has seen a dramatic increase in interest in new detection technologies. Today single-photon detectors are widely used in various fields of science and high technologies, namely in quantum cryptography, quantum communication, telecommunications, generation of optical quantum states and quantum random numbers, astrophysics, elementary particle physics, biology and medicine, chemistry and spectroscopy, metrology and others [1-4]. The creation of detectors with improved characteristics will expand the range of tasks for the solution of which they can be used. A thermoelectric single-photon detector (TSPD) can compete with existing detectors [5-10]. In our previous studies, we have shown that the TSPD count rates can exceed the record values achieved by detectors with other designs [11-14]. At the same time, TSPD has high energy resolution and photon detection efficiency in a wide range of the electromagnetic spectrum. In these works cerium-doped lanthanum hexaboride ($La_{1-x}Ce_xB_6$) and cerium hexaboride (CeB_6) were used as a sensor of thermoelectric detector, that have high thermoelectric properties at 0.5 K and 9 K respectively. It is obvious that low operating temperatures of single-photon detectors are necessary to suppress the thermal noise. This requirement leads to the necessity of using in TSPD compounds having high Seebeck coefficient at low temperatures. In [15-16] we present the results of computer simulation of heat distribution processes taking place after the absorption of single photons of 1 – 1000 eV energy in detection pixel of TSPD, containing $FeSb_2$ strongly correlated semiconductor sensor. The investigation results of three-layer detection pixel of TSPD with $FeSb_2$ sensor are stated in [15] and those of single layer detection pixel in [16]. The present work is the continuation of already realized researches.

2. Methodology

The TSPD three-layer detection pixel has simple design and provides the possibility to create detector matrix with simple electronic structure. Fig. 1 shows the general view of the detection pixel. As a material for the absorber and heat sink, we have chosen tungsten (W), and for thermoelectric sensor – strongly correlated semiconductor $FeSb_2$.

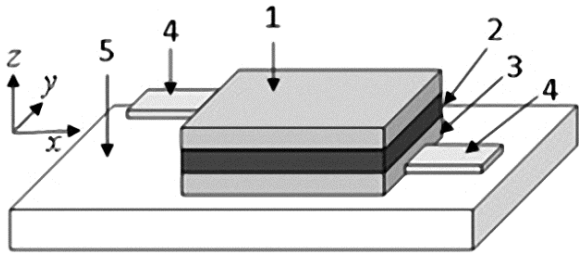

Fig. 1. Three-layer detection pixel design:
1 – absorber; 2 – thermoelectric sensor; 3 – heat sink;
4 – contacts to low temperature electronic; 5 – substrate.

The physical parameters of CeB_6 and $FeSb_2$ thermoelectrics at 9 K are presented in Table 1 in accordance to the data of papers [17-21]. It can be seen that $FeSb_2$ has significantly greater Seebeck coefficient that will provide much larger voltage, appearing on the sensor for the same temperature difference on the sensor boundaries (Fig. 2). $FeSb_2$ also possesses higher thermal conductivity and lower heat capacity, in comparison to CeB_6. Accordingly, the processes of heat propagation in the detection pixels will proceed in a completely different manner, when using these two thermoelectrics. The propagation of heat (released at the photon absorption in absorber) in the detection pixel with $FeSb_2$ sensor should occur faster.

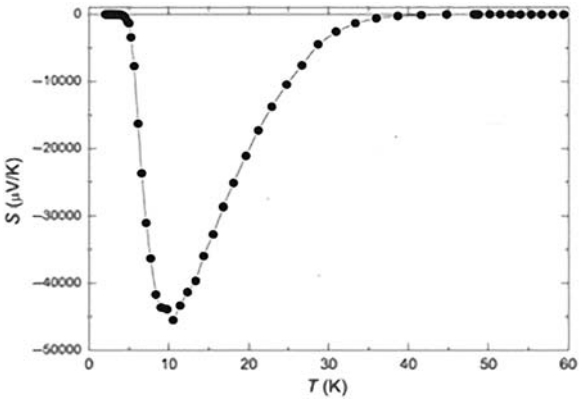

Fig. 2. Thermopower of $FeSb_2$ vs. temperature [22].

For the same geometric dimensions of the detection pixels, in the case of $FeSb_2$, the decrease in the temperature difference at the sensor boundaries and the increase in the counting rate can be expected. A smaller value of the temperature difference at the sensor boundaries means a smaller signal-to-noise ratio, which, however, must be compensated by large values of voltage on the sensor. At the same time, in order to obtain optimal detector characteristics, the thickness of the sensor can be varied for each thermoelectric.

The calculations of the heat propagation processes in the three-layer detection pixel containing $FeSb_2$ sensor were carried out by a procedure similar to that, described in [11, 13]. The calculations were based on heat conduction equation and were carried out by the matrix method for differential equations.

Table 1. Physical parameters of $FeSb_2$ and CeB_6 at 9 K.

Parameter, unit	Compound	
	$FeSb_2$	CeB_6
Density, kg/m^3	8170	4800
Specific heat capacity, J/kg·K	0.0133	0.196
Thermal conductivity, W/m·K	500	0.94
Seebeck coefficient, μV/K	-42000	150

The thermal processes were modeled according to the following algorithm.

- The entire volume of the absorber and the bridge was broken down into the cells with the dimensions Δx, Δy and $\Delta z \leq 0.1$ μm. Obviously, the enlargement of the number of cells will provide more accurate calculations, but it will lead to more time consuming.
- The initial temperature for the all cells was set 9 K. In the absorber was chosen the cell where the photon is absorbed.
- According to the formula $\Delta T = E / V \cdot \rho \cdot c$, where E is the energy of the absorbed photon and V is the cell volume, the initial temperature of the cell $T_0 = 9\ \text{K} + \Delta T$ was calculated.

3. Results

As the thickness of the absorber is the most important parameter of the TSPD sensor, selecting this parameter we were proceeding from the demand to provide high probability of photon absorption in the absorber. It is easy to calculate that the probability of absorption of 1 keV energy photon in 1.5 μm thick W will be 0.9998 applying the Bouguer-Lambert law and using 5.775 μm^{-1} value for the coefficient of linear attenuation in W [23]. Absorption probability will exceed 0.9999 for 100 eV and 10 eV photons in 0.5 μm and 0.1 μm thick W respectively. It can be noted that thinner tungsten absorbers or absorbers fabricated from not heavy metals can be used for the absorption of photons with energies less than 10 eV with the same probability.

The geometrical dimensions of sensors and results of calculations of heat propagation in W/$FeSb_2$/W three-layer sensor are presented in Table 2. The

columns in the table give the calculation number, the thickness of absorber (Z_1), the thickness of thermoelectric layer (Z_2), the thickness of heat sink (Z_3), the photon energy (E), the maximum temperature difference on the thermoelectric sensor after photon absorption – (ΔT_m), time duration to achieve the ΔT_m – (t_m), the maximum of voltage on the sensor (V_m), the time of recession ΔT to the background 10^{-4} K – (t_b), its inverse (count rate) – (R).

Table 2. W/$FeSb_2$/W three-layer detection pixel geometry, photon energy and calculated parameters.

No	Z_1, μm	Z_2, μm	Z_3, m	E, eV	ΔT_m, 10^{-4} K	t_m, ps	V_m, μV	t_b,ps	R, GHz
FeSb1	0.5	1	1	100	130	0.009	546	0.36	2778
FeSb2	0.5	0.5	1	100	124	0.009	521	0.25	4000
FeSb3	0.5	0.1	1	100	8.49	0.006	35.7	0.042	23810
FeSb4	0.5	0.01	1	100	0.09	0.0045	0.4	-	-
FeSb5	0.5	1	1	110	143	0.009	601	0.37	2703
FeSb6	0.5	1	1	101	131	0.009	550	0.36	2778
FeSb7	0.1	1	1	11	1122	0.0015	4712	0.37	2703
FeSb8	0.1	1	1	10	1020	0.0015	4284	0.36	2778
FeSb9	0.1	1	1	7	714	0.0015	2999	0.3	3333
FeSb10	0.1	1	1	4	408	0.0015	1714	0.22	4545
FeSb11	0.1	1	1	1.1	112	0.0015	470	0.15	6667
FeSb12	0.1	1	1	1	102	0.0015	428	0.108	9259
FeSb13	0.1	1	1	0.9	92	0.0015	386	0.102	9804
FeSb14	1.5	1	1	1000	516	0.015	2167	0.93	1075
FeSb15	1.5	1	1	1010	522	0.015	2192	0.96	1041
FeSb16	1.5	1	1	1100	568	0.015	2386	0.99	1010
FeSb17	0.1	1	1	0.1	10.2	0.0015	42.8	0.0249	40160
FeSb18	0.1	1	1	0.09	9.18	0.0015	38.6	0.0228	43860
FeSb19	0.1	0.5	1	1	102	0.0015	428	0.0717	13947
FeSb20	0.1	0.1	1	1	36	0.0009	151	0.0075	133333
FeSb21	0.1	2	1	1	102	0.0015	428	0.1503	6653
FeSb22	0.1	3	1	1	102	0.0015	428	0.1629	6139
FeSb23	0.5	2	1	100	130	0.009	546	0.51	1960
FeSb24	0.5	3	1	100	130	0.009	546	0.63	1587
FeSb25	0.5	4	1	100	130	0.009	546	0.72	1389
mFe26M	0.5	0.5	2	100	124	0.009	521	0.243	4115
mFe27M	0.5	0.5	0.5	100	124	0.009	521	0.303	3300
mFe28M	0.5	0.5	0.25	100	125	0.009	525	0.315	3175
mFe29M	0.5	0.5	0.1	100	125	0.009	525	0.303	3300

In accordance with Fig. 1, the geometric dimensions X and Y of the thermoelectric sensor and heat sink are similar to those of absorber and equal to 10 μm. In all calculations, it was assumed that the photon is thermalized in the center of the absorber surface and the thickness of tungsten heat sink is 1 μm.

We shall start the discussion of the obtained results with consideration of absorption of hard UV photon with 100 eV energy. Let us investigate the temporal behavior of the temperature difference ΔT(t) between two surfaces of the thermoelectric sensor in its four different parts that are at different distances from the sensor center. The graphs of this dependence for the calculation FeSb1 from Table 2 are given in Fig. 3. As expected, the highest values for the temperature difference are reached in the center of the sensor, directly under the point of photon thermalization. With distancing from the center, the signal weakens and in the point 4 (which is the farthest) the maximum is reached in 1.6 ps from the moment of photon absorption and is lower from the background value. A similar result can be seen for the rest of calculations, and since the value of arising voltage on the sensor is

determined by the maximal temperature difference on the thermoelectric layer, we shall further consider only the dependences ΔT(t) calculated for the region 1.

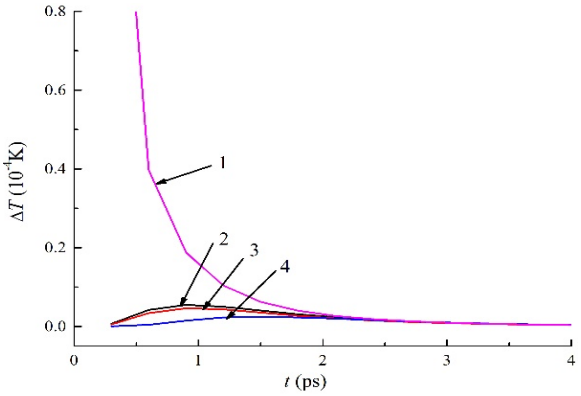

Fig. 3. $\Delta T(t)$ dependence of the calculation FeSb1 measured in five different areas of the thermoelectric sensor: in the center (1), at different distances from the center: 0.5 μm (2), 1 μm (3), 5 μm (4).

For more clear representation of the parameters ΔT_m, t_m and t_b given in Table 2, they are denoted in Fig. 4, which shows $\Delta T(t)$ dependence for the calculation of FeSb1, starting from the moment of absorption of the photon in the absorber until the signal falls to the background value.

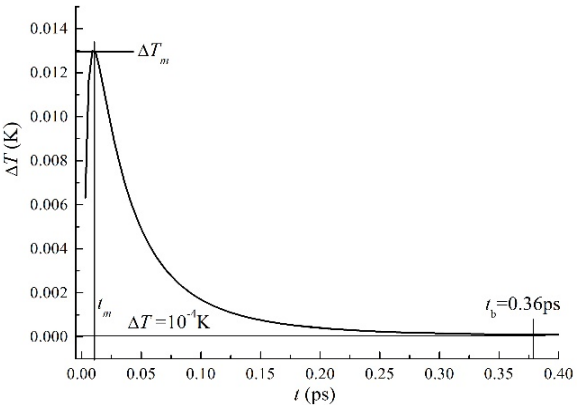

Fig. 4. $\Delta T(t)$ dependence of the calculation FeSb1 measured in the center of the thermoelectric sensor

Temporal dependence of ΔT parameter of the calculations FeSb1 – FeSb3 is presented on Fig. 5. The observed difference in the course of $\Delta T(t)$ dependencies shows that the characteristics of the detection pixel vary significantly with the change in the thickness of $FeSb_2$ sensor.

Fig. 6 shows the dependence of the parameters ΔT_m and R on the thickness of the sensor for calculations FeSb1 – FeSb4 and FeSb23 – FeSb25 corresponding to the absorption of 100 eV energy photon. The parameter ΔT_m does not change and the counting rate slightly increases when the thickness of the sensor is reduced from 4 μm to 1 μm. With smaller sensor thicknesses, the parameter ΔT_m sharply decreases and at the thickness of 0.01 μm it becomes much smaller than the background value 10^{-4} K. The parameter R reaches tens of terahertz.

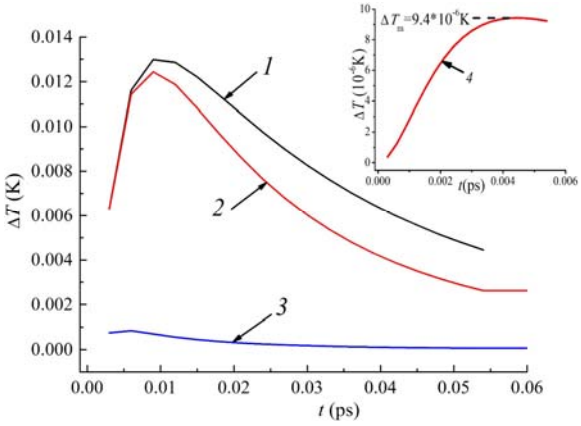

Fig. 5. $\Delta T(t)$ dependence of the calculations: *1* – FeSb1, *2* – FeSb2, *3* – FeSb3, in insert *4* – FeSb4.

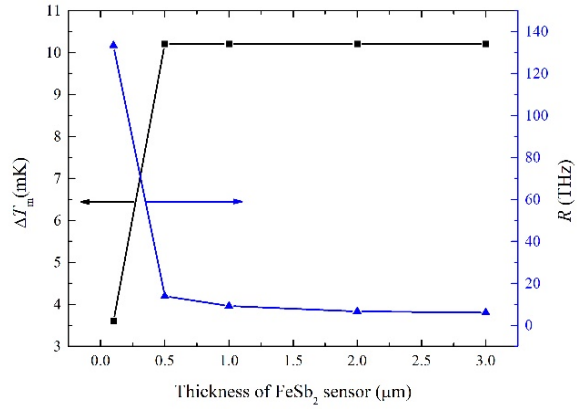

Fig. 6. ΔT_m and R parameters vs thickness of $FeSb_2$ layer for 100 eV energy photons.

Fig. 7 shows $V(t)$ graphs for the cases of 100 eV, 110 eV and 101 eV energy photons' absorption (calculations FeSb1, FeSb5 and FeSb6) in the detection pixels with the same sensor thickness equal to 1 μm. It can be seen that the change of photon energy leads to the change in V_m value, while t_m does not change. It follows from Table 2 that V_m values differ by 47 μV, if the photon energies differ by 10 %, and by 4 μV, if they differ by 1 %. It should also be mentioned that the change in photon energy leads to the some change of the count rate. The parameter R is smaller in the case of higher photon energies, since after the thermalization of a higher energy photon the temperature difference resulting on the thermoelectric layer is slowly going down to the background value.

Calculations presented in Table 2 for 11 eV and smaller photon energies were done for the sensor with 0.1 μm absorber thickness.

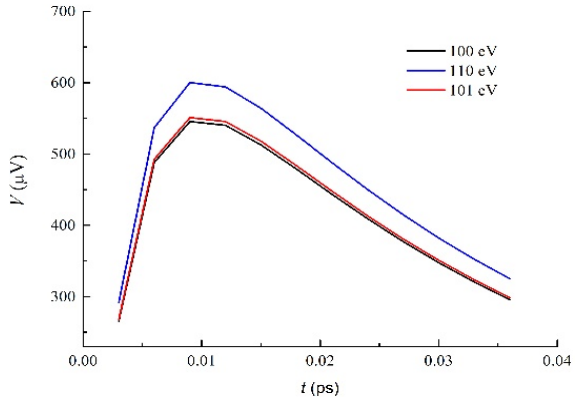

Fig. 7. Voltage on sensor temporal dependences of calculation numbers FeSb1, FeSb5 and FeSb6 for the cases of absorption of photons with 100 eV, 110 eV and 101 eV energies.

The parameters ΔT_m and R obtained as a result of calculations for the absorption of photons with energies of 11 – 0.09 eV are shown in Fig. 8. These values of photon energies correspond to a very important area of the electromagnetic spectrum from IR to UV.

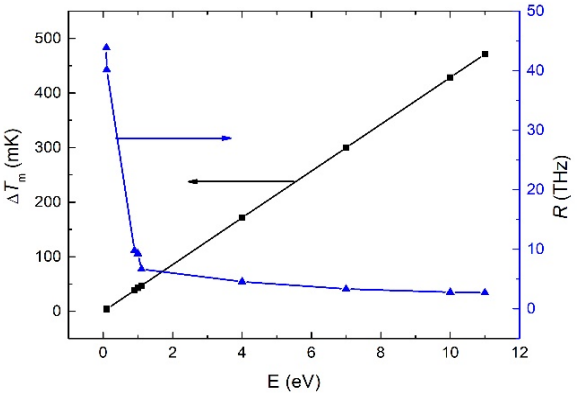

Fig. 8. ΔT_m and R parameters for 0.09 – 11 eV photons.

While increasing the photon energy, the parameter ΔT_m increases linearly, which is a very important characteristic of the detector, and makes it possible to determine the photon energy using the maximum of the signal that appears on the sensor.

As follows from the data of Table 2 and Fig. 8, we have received a very large signal for all these energies. The parameter ΔT_m varies within the range of 9.2 – 122.2 mK with an energy change from 0.9 eV to 11 eV. The parameter V_m for the same photon energies assumes values of 0.386 – 4.712 mV. At the level of 10 eV and 1 eV, the photon energy change by 10% leads to the change in the parameter V_m by 688 μV and 42 μV respectively.

In this energy range, the counting rate is smaller in calculations carried for high energies. However, for all energy photons' the counting rate reaches terahertz and varies within 2.7 - 43.8 THz.

Fig. 9 shows the dependences of the parameters ΔT_m and R on the thickness of the sensor for FeSb12 and FeSb19 – FeSb22 calculations that correspond to the absorption of 1 eV energy photon.

The presented graphs are similar to the graphs in Fig. 6, but the results of calculations for the 0.1 μm thick sensor differ significantly. From the calculations for 1 eV energy photons' absorption, we have a signal much greater than the background level and the count rate more than one hundred terahertz. Note also, that the parameter ΔT_m does not change its value when the sensor thickness varies from 3 μm to 0.5 μm.

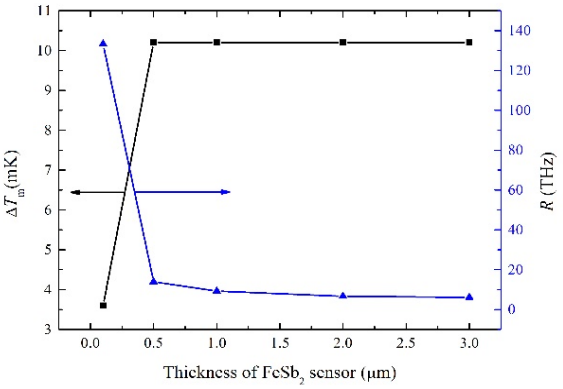

Fig. 9. ΔT_m and R parameters vs thickness of the $FeSb_2$ layer for photons with energy of 1 eV.

Let's consider how the characteristics of the sensor change in the case of the absorption of infrared photons with energy of about 0.1 eV. FeSb17 and FeSb18 calculations show that the signal for these energies exceeds the background value for 10 times, that is a good result. The parameter V_m differs by 4.2 μV when the energy differs by 10 %. Registration of signals differing by 0.4 μV will prove the achievement of 1 % energy resolution on 0.1 eV level. The counting rate, obtained from these calculations, is also very high.

Let us consider the results of calculations for ~ 1 keV energy X-ray photons' absorption. The calculations were done for the detection pixel with 1.5 μm absorber thickness. Fig. 10 shows $\Delta T(t)$ dependences in accordance to FeSb14 – FeSb16 calculations.

It can be seen that for X-ray photons the energy change leads to the change in ΔT_m value, while t_m does not change. The same result was obtained also for UV photons (Fig. 6). It follows from Table 2 that V_m values differ by 219 μV if the photon energies differ by 10 %, and by 25 μV, if they differ by 1 %. The count rate for X-ray photons varies from 1010 GHz to 1075 GHz.

In conclusion, let us compare the results of calculations mFe2M, mFe26M – mFe26M for sensors with 0.1 – 2 μm thicknesses of W heat sink. It is seen from Table 2 that the variation of the heat sink thickness does not influence the value of parameter ΔT_m, but the count rate changes slightly from 4.1 THz to 3.1 THz (Fig. 11). It can be concluded that the

thickness of the heat sink does not have significant influence on the characteristics of the detection pixel, so it can be selected taking into account other demands of the construction.

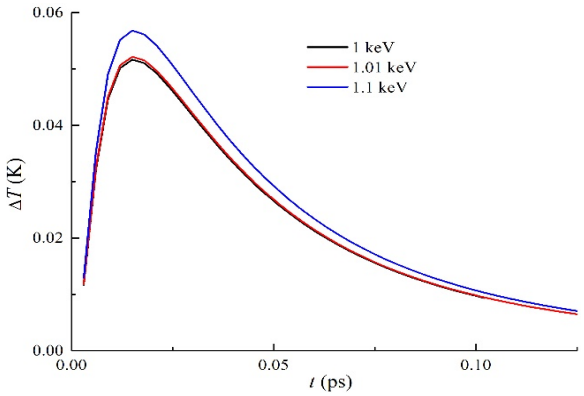

Fig. 10. $\Delta T(t)$ dependences of calculation numbers FeSb14 – FeSb16 for the cases of absorption of photons with 1 keV, 1.01 keV and 1.1 keV energies.

The comparison of the computer simulation data of heat propagation processes in the three-layer detection pixel of thermoelectric detector, that contains CeB_6 and $FeSb_2$ sensors, is presented in Table 3. The main parameters of the sensors obtained from the calculations for various energies of the absorbed photons are given in the table. The calculation data for the same geometric dimensions of the detection pixels' surfaces, the same absorber thickness and the optimal thickness of the thermoelectric layer are compared.

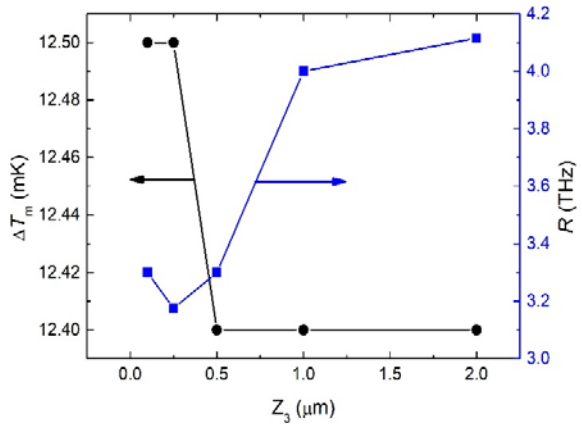

Fig. 11. ΔT_m and R parameters vs thickness of the W heat sink for photons with energy of 100 eV.

The comparison of the calculation parameters for CeB_6 and $FeSb_2$ sensors shows, that for $FeSb_2$ sensor the parameter ΔT_m is larger by an order of magnitude for 1 keV energy photons, is three times smaller for 100 eV energy photons and for 10 eV and 1 eV energy photons has close values. However, the maximum electrical voltage that appears on the sensor, as well as the counting rate, are much larger for the whole considered energy interval of 1 eV – 1 keV.

Table 3. Calculation parameters for 1 – 1000 eV photon absorption in the three-layer detection pixels of TSPD containing CeB_6 and $FeSb_2$ sensors.

***E*, eV**	**ΔT_m, mK**		**V_m, μV**		***R*, GHz**	
	CeB_6	**$FeSb_2$**	**CeB_6**	**$FeSb_2$**	**CeB_6**	**$FeSb_2$**
1000	5.64	51.6	0.846	2167	208	1075
100	33.71	13	5.056	546	337	2778
10	114.7	102	17.2	4284	758	4545
1	11.5	10.2	1.725	428	3300	9259

4. Conclusions

The results of computer simulation of heat distribution processes taking place after absorption of single photons from IR to X-ray in three-layer $W/FeSb_2/W$ detection pixel of the thermoelectric detector are being analyzed. Different geometries of the detection pixel with tungsten absorber, thermoelectric layer of $FeSb_2$ and tungsten heat sink are considered.

The obtained results allow the following conclusions to be done:

1) The three-layer $W/FeSb_2/W$ detection pixel of TSPD may register individual photons in a wide range of the electromagnetic spectrum from 0.09 eV to 1.1 keV, providing energy resolution of not less than 1 % and count rate from one to hundred terahertz.

2) The maximum voltage on $FeSb_2$ sensor of TSPD can reach millivolts when registering single photon absorption.

3) Taking into account several features of the detection pixel of thermoelectric detector, such as simple design, high position resolution and absence of strict requirements to operating conditions, it can be argued that thermoelectric detectors with $FeSb_2$ sensor can be a real competitor to superconducting detectors.

This work can find continuation in the studies of the characteristics of TSPD detection pixel with $FeSb_2$

thermoelectric layer, superconducting absorber and heat sink. As shown in [24-26], the superconducting absorber and the heat sink provide additional advantages to thermoelectric detector in comparison with other single-photon detectors.

Acknowledgements

The author would like to thank Dr. A. M. Gulian for the helpful discussions and is grateful to A. A. Kuzanyan and V. R. Nikoghosyan for their help in calculation fulfillment.

References

[1]. T. Yamashita, S. Miki, H. Terai, Recent Progress and Application of Superconducting Nanowire Single-Photon Detectors, *IEICE Transactions on Electronics*, Vol. E100-C, Issue 3, 2017, pp. 274-282.

[2]. R. H. Hadfield, Single-photon detectors for optical quantum information applications, *Nature Photonics,* Vol. 3, Issue 12, 2009, pp. 696-705.

[3]. J. J. Renema, Q. Wang, R. Gaudio, I. Komen, K. Hoog Op'T, D. Sahin, A. Schilling, M. P. van Exter, A. Fiore, A. Engel, M. J. A. de Dood, Position-Dependent Local Detection Efficiency in a Nanowire Superconducting Single-Photon Detector, *Nano Letters,* Vol. 15, Issue 7, 2015, pp. 4541-4545.

[4]. N. A. Tyler, J. Barreto, G. E. Villarreal-Garcia, D. Bonneau, D. Sahin, J. L. O'Brien, M. G. Thompson, Modelling superconducting nanowire single photon detectors in a waveguide cavity, *Optics Express*, Vol. 24, Issue 8, 2016, pp. 8797-8808.

[5]. G. G. Fritz, K. S. Wood, D. van Vechten, A. L. Gyulamiryan, A. S. Kuzanyan, N. J. Giordano, T. M. Jacobs, H.-D. Wu, J. S. Horwitz, A. M. Gulian, Thermoelectric single-photon detectors for X-ray/UV radiation, *Proceedings of SPIE*, Vol. 4140, 2000, pp. 459-469.

[6]. D. Van Vechten, K. Wood, G. Fritz, J. Horwitz, A. Gyulamiryan, A. Kuzanyan, V. Vartanyan, A. Gulian, Imaging detectors based on anisotropic thermoelectricity, *Nuclear Instruments and Methods in Physics Research*, Vol. 444, Issue 1-2, 2000, pp. 42-45.

[7]. A. Gulian, K. Wood, D. Van Vechten, G. Fritzdet, Cryogenic Thermoelectric (QVD) Detectors: Emerging Technique for Fast Single-photon and Non-dispersive Energy Characterization, *Journal of Modern Optics*, Vol. 51, Issue 9-10, 2004, pp. 1467-1490.

[8]. K. Wood, D. Van Vechten, G. Fritz, H.-D. Wu, S. Bounnak, K. Bussman, K. Winzer, S. Kunii, V. Gurin, M. Korsukova, C. Mitterer, M. Corlsson, F. Golf, A. Kuzanyan, G. Badalyan, S. Horutyunyan, S. Petrosyan, V. Vardanyan, T. Paronyan, V. Nikoghosyan, A. Gulian, Toward Ultimate Limits of Performance of the QVD Detector, *Nuclear Instruments and Methods in Physics Research*, Vol. 520, Issue 1-3, 2004, pp. 56-59.

[9]. A. Gulian, K. Wood, D. VanVechten, G. Fritz, H.-D. Wu, S. Bounnak, K. Bussman, K. Winzer, S. Kunii, V. Gurin, M. Korsukova, C. Mitterer, M. Corlsson, F. Golf, A. Kuzanyan, G. Badalyan, S. Horutyunyan, S. Petrosyan, V. Vardanyan, T. Paronyan, V. Nikoghosyan, Current developmental status of thermoelectric (QVD) detectors, *Nuclear Instruments and Methods in Physics Research*, Vol. 520, Issue 1-3, 2004, pp. 36-40.

[10]. V. A. Petrosyan, Hexaborides of Rare Earths as a Sensor Material for Thermoelectric Single-Photon Detectors, *J. Contemp. Phys. (Arm. Acad. Sci.)*, Vol. 46, 2011, Issue 3, pp. 125-129.

[11]. A. S. Kuzanyan, V. R. Nikoghosyan, A. A. Kuzanyan, Modeling of Kinetic Processes in Thermoelectric Single-photon Detectors, *Proceedings of SPIE*, Vol. 9504, 2015, pp. 95040O-1 - 95040O-10.

[12]. A. S. Kuzanyan, V. R. Nikoghosyan, A. A. Kuzanyan, CeB_6 Sensor for Thermoelectric Single-Photon Detector, *Sensors & Transducers*, Vol. 191, Issue 8, August 2015, pp. 57-62.

[13]. A. A. Kuzanyan, V. R. Nikoghosyan, A. S. Kuzanyan, Ultra-fast Sensor for Single-photon Detection in a Wide Range of the Electromagnetic Spectrum, *Sensors & Transducers*, Vol. 207, Issue 12, December 2016, pp. 21-29.

[14]. A. A. Kuzanyan, Computer Simulation of Heat Distribution Processes in W/$(La,Ce)B_6$/W Sensor of Thermoelectric Detector, *Journal of Contemporary Physics (Armenian Academy of Sciences)*, Vol. 51, Issue 4, 2016, pp. 360-370.

[15]. A. A. Kuzanyan, V. R. Nikogosyan, A. S. Kuzanyan, Strongly correlated semiconductor FeSb2 as a sensor of single photon thermoelectric detector, in *Proceedings of the Conference on 3rd International Conference on Sensors and Electronic Instrumentation Advances (SEIA 2017)*, Moscow, Russia, 20-22 September 2017, pp. 163-168.

[16]. A. A. Kuzanyan, V. R. Nikoghosyan, A. S. Kuzanya, Investigation of the processes of heat propagation in W/$FeSb_2$/W detection pixel of the single photon thermoelectric detector, *Journal of Contemporary Physics (Armenian Academy of Sciences)*, Vol. 52, Issue 3, 2017, pp. 249-257.

[17]. A. A. Kuzanyan, A. S. Kuzanyan, V. R. Nikoghosyan, V. N. Gurin, M. P. Volkov, Investigation of processes of heat propagation in multilayer sensor of thermoelectric single-photon detector, *Journal of Contemporary Physics (Armenian Academy of Sciences)*, Vol. 51, Issue 2, 2016, pp. 181-190.

[18]. S. R. Harutyunyan, V. H. Vardanyan, A. S. Kuzanyan, V. R. Nikoghosyan, S. Kunii, K. S. Wood, A. M. Gulian, Thermoelectric Cooling at Cryogenic Temperatures, *Appl. Phys. Letter*, Vol. 83, Issue 11, 2003, pp. 2142-2144.

[19]. Springer Materials Web Portal (http://materials.springer.com/isp/crystallographic/docs/sd_1008518).

[20]. M. S. Figueira, J. Silva-Valencia, R. Franco, Thermoelectric properties of the Kondo insulator $FeSb_2$, *European Physical Journal B,* Vol. 85, No. 203, 2012, pp. 1-9.

[21]. A. Bentien, S. Johnsen, G. K. H. Madsen, B. B. Iversen, F. Steglich, Colossal Seebeck coefficient in strongly correlated semiconductor $FeSb_2$, *Europhysics Letters*, Vol. 80, No. 1, 2007, pp. 17008-1 – 17008-5.

[22]. N. Oeschler, S. Hartmann, U. Köhler, M. Deppe, P. Sun, F. Steglich, Thermoelectric Power of Correlated Compounds, in Properties and Applications of Thermoelectric Materials, Eds. V. Zlatic, A. C. Hewson, in *Proceedings of the Conference on 'NATO Advanced Research Workshop on Properties and Applications of Thermoelectric*

Materials', Hvar, Croatia 21-26 September 2008, pp. 81-90.
[23]. C. T. Chantler, Theoretical Form Factor, Attenuation and Scattering Tabulation for Z=1-92 from E=1-10 eV to E=0.4-1.0 MeV, *Journal of Physical and Chemical Reference Data,* Vol. 24, Issue 1, 1995, pp. 71-643.
[24]. A. S. Kuzanyan, A. A. Kuzanyan, V. R. Nikoghosyan, Multilayer sensor of thermoelectric detector, *Patent of Armenia № A3043,* 2016, pp. 1-12.
[25]. A. A. Kuzanyan, V. R. Nikoghosyan, A. S. Kuzanyan, An ultra-fast thermoelectric sensor for single-photon detection in a wide range of the electromagnetic spectrum, *Proceedings of SPIE*, Vol. 10229, 2017, pp. 102290P-1 – 102290P-9.
[26]. A. S. Kuzanyan, A. A. Kuzanyan, V. R. Nikoghosyan, Superconductor /Thermoelectric/ Superconductor Heterostructure for Single-photon detection, in *Book of Abstract of the Conference on Laser Physics,* Ashtarak, Armenia, 19-22 September 2017, pp. 61-62.

Published by International Frequency Sensor Association (IFSA) Publishing, S. L., 2017 (http://www.sensorsportal.com).